2013

Studies of the surface reaction mechanisms of Pb-3 wt%Sn-0.5 wt%Ag anode in CrO3 solutions

Jianzhong Li
Northeastern University, China

Xiuli Sun
Northeastern University, China

Yanwen Tian
Northeastern University China

Yue Zhao
University of Wollongong, yue@uow.edu.au

Publication Details

Li, J., Sun, X., Tian, Y. & Zhao, Y. (2013). Studies of the surface reaction mechanisms of Pb-3 wt%Sn-0.5 wt%Ag anode in CrO3 solutions. Journal Of The Electrochemical Society, 160 (6), E60-E66.

Studies of the surface reaction mechanisms of Pb-3 wt%Sn-0.5 wt%Ag anode in CrO3 solutions

Abstract
This work examines the change of surface properties and the reaction process of lead alloy anode in CrO3 solution under conditions of high current density, by means of SEM, EDX, XRD, electrochemical test and Raman spectroscopy, for understanding the corrosion mechanism of lead alloy anode. In the initial oxidation stage of lead alloy anode, the diffraction peaks of monoclinic PbCrO4 and PbO are clearly shown in the XRD spectrum of the lead alloy surface. With increasing reaction time, PbCrO4 and PbO diffraction peaks are weakened and those of lead dioxide strengthened. Cyclic voltammetry reveals that the electrode potential change is among Pb, PbO, PbCrO4, PbO1+x (0 < x < 1) and beta-PbO2. According to impedance tests, charge transfer and a corrosion product film on lead alloy surface happen under the high and medium frequencies, and chromium-oxide ion clusters are absorbed on free sites of the anode surface for the low frequency. The corrosion products have characteristic of complex semiconducting behavior shown in the Mott-Schottky plots. Raman spectra indicates that Cr2O72- and HCrO4- ions are firstly absorbed on the anode surface, and then PbCrO4 is produced between Cr2O72- and Pb, PbO is reacted from HCrO4-. The mechanism of the anode reaction at the anode/solution interface is discussed using the experimental results.

Keywords
cro3, anode, ag, 5, sn, solutions, wt, studies, 3, pb, mechanisms, reaction, surface

Disciplines
Engineering | Science and Technology Studies

Publication Details
Li, J., Sun, X., Tian, Y. & Zhao, Y. (2013). Studies of the surface reaction mechanisms of Pb-3 wt%Sn-0.5 wt%Ag anode in CrO3 solutions. Journal Of The Electrochemical Society, 160 (6), E60-E66.

Journal of The Electrochemical Society, **160** (6) E60-E66 (2013)
0013-4651/2013/160(6)/E60/7/$31.00 © The Electrochemical Society

Studies of the Surface Reaction Mechanisms of Pb-3 wt%Sn-0.5 wt%Ag Anode in CrO_3 Solutions

Jianzhong Li,[a,z] Xiuli Sun,[a] Yanwen Tian,[a] and Yue Zhao[b]

[a]*School of Materials and Metallurgy, Northeastern University, Shenyang 110819, China*
[b]*MMM School, Faculty of Engineering, University of Wollongong, NSW 2522, Australia*

This work examines the change of surface properties and the reaction process of lead alloy anode in CrO_3 solution under conditions of high current density, by means of SEM, EDX, XRD, electrochemical test and Raman spectroscopy, for understanding the corrosion mechanism of lead alloy anode. In the initial oxidation stage of lead alloy anode, the diffraction peaks of monoclinic $PbCrO_4$ and PbO are clearly shown in the XRD spectrum of the lead alloy surface. With increasing reaction time, $PbCrO_4$ and PbO diffraction peaks are weakened and those of lead dioxide strengthened. Cyclic voltammetry reveals that the electrode potential change is among Pb, PbO, $PbCrO_4$, PbO_{1+x} $(0 < x < 1)$ and β-PbO_2. According to impedance tests, charge transfer and a corrosion product film on lead alloy surface happen under the high and medium frequencies, and chromium-oxide ion clusters are absorbed on free sites of the anode surface for the low frequency. The corrosion products have characteristic of complex semiconducting behavior shown in the Mott–Schottky plots. Raman spectra indicates that $Cr_2O_7^{2-}$ and $HCrO_4^-$ ions are firstly absorbed on the anode surface, and then $PbCrO_4$ is produced between $Cr_2O_7^{2-}$ and Pb, PbO is reacted from $HCrO_4^-$. The mechanism of the anode reaction at the anode/solution interface is discussed using the experimental results.
 [DOI: 10.1149/2.105306jes]

Manuscript submitted March 5, 2013; revised manuscript received March 25, 2013. Published April 4, 2013.

Lead and its alloys have good castability and mechanical properties, low corrosion rates, high electrocatalytic efficiency and good conductivity of the contact layer.[1,2] So, lead and its alloys have been widely used in industrial applications such as chromium plating,[3] electrochemistry surface passivation,[4] lead/acid batteries,[5,6] and hydrometallurgical processes (e.g. zinc electrowinning).[7,8] In these applications, lead-alloy anodes undergo high current densities, in aggressive environments, such as sulphuric acid, CrO_3 solution or fluoride-included solution. A layer of lead oxide or dioxide is easily found on lead-alloy anodes surface during use, which is essential because the PbO_2 layer is the electrochemically active component of the anode. However, after practical application the dioxide layer has a tendency to crack or break from the lead-alloy anode, exposing the underneath fresh lead surface to the electrolyte. This causes the anode corrosion and leads to contamination in the products, increase in energy consumption and material/labor costs due to the need for periodical maintenance.[9,10]

Corrosion of lead-alloy anodes is not only related with lead alloy properties, but also with the application environment. Numerous previous investigations[11–15] aiming for the improvement of Pb anodes' corrosion resistance focus on the inclusion of various alloying additives in the lead anode to achieve better mechanical properties and/or finer-grained and more homogeneous microstructure. In addition, corrosion mechanism of the lead-alloy has been intensively investigated in sulphuric acid solutions.[13–15] For anode in solution containing chromium, some researches indicate that the alloying additions in lead base alloys anode affect the microstructure and electrochemical characteristics of active materials,[16] corrosion rate[17] and layers structure[18] on the electrode. However, few reports regarding anode surface action in the more aggressive (strong oxidation and high acidity) environment of CrO_3 solution at high current densities of above 10 A/dm^2 are available in literature. Under these conditions, lead-alloy anodes degrade more rapidly than in the other solutions.

The aim of the present work is to study the change in surface structure and reaction mechanism of a typical lead-alloy anode in CrO_3 solutions and to determine the effect of higher current density and chrome ion concentration on the corrosion of the lead alloy. Pb-Sn (Pb-Ag) alloy anode[6,8–12] is widely used/recently developed for lead-alloy anode applications. It is important to improve the corrosion resistance of the lead alloy anodes with optimum plating conditions for the chromium plating industry, and the results will also help in understanding the electrode dynamic process in the lead alloy/CrO_3 solution system.

[z]E-mail: lijz@smm.neu.edu.cn

Experimental

Sample preparation.— The substrate material used in the research was a Pb-3 wt%Sn-0.5 wt%Ag ingot-cast alloy for commercial anode applications in tin free steel field (i.e., tin free steel refers to the steel electroplated with chromium instead of tin on its surface, which can be used as the substitution of tinplating in various industrial applications).[19] Rectangular substrates with dimensions of 50 mm × 40 mm × 8 mm were used in the research. The substrates were mechanically polished with emery papers up to 1000 grit to ensure similar surface roughness. The polished substrates were thoroughly washed with acetone and distilled water before passing through the plating procedure as the anode. CrO_3 solutions were used as electrolytic solutions, which is made of chemical pure chromic anhydride as solute with its concentrations of 130, 150 and 170 g/L, respectively. The concentration range is varied practically in tin free steel field. A low carbon steel was used as cathode to set up electrolysis system for preparing the sample under the different conditions. The same set of electrolysis experiments was carried out over the oxidation time of 15, 30, 60 min and 10, 30, 60s and current density of 10, 20, 30 A/dm^2, respectively.

Analysis of surface properties.— Morphology of the oxidation coatings was analyzed using a scanning electron microscope. The energy dispersive X-ray spectroscopy analysis was used for determining the content of the oxidation coatings. Crystallinity of the oxidation coatings was investigated using a Rigaku D/ max-rA X-ray diffractometer. X-ray profiles were measured between 10 and 80 deg. (2μ angle) at 45 kV and 40 mA with Cu K-alpha radiation source. The scanning speed and space length were 8 deg./min and 0.02 deg., respectively.

Electrochemical test.— Cyclic voltammetric, AC impedance and Mott–Schottky measurements were performed in a conventional 250 mL three-compartment Pyrex cell using electrochemical workstation, model PARSTAT 2273(American Princeton Company). A defined sample area of 2 cm^2 was exposed to the electrolyte, and all the current value was normalized to the geometrical surface area. A luggin capillary was placed near the working electrode to minimize the solution resistance. A platinum foil was used as counter electrode for evaluating the electrochemical properties of the oxide films, and a saturated calomel electrode (SCE) was used as reference electrode. All electrode potentials were referred to SCE if no otherwise stated. Cyclic voltammetry tests were carried out at room temperature (25 ± 1°C) with a potential range between −1.5 V to 2 V with the frequency of 1000 Hz and sweep rate of 2 mV.s^{-1}. Electrochemical

impedance spectroscopy measurements were performed in a frequency range of 10^5 Hz to 10^{-1} Hz with ten points per decade and a sine wave with 10 mV amplitude was used to perturb the system. The impedance data were analyzed and fitted with the Zsimpwin equivalent-circuit simulation software. A high potential sweep rate of 50 mV/s was used in the Mott–Schottky measurements in order to avoid the polarizing effect on passive film, especially in the high over-potential region, which is potential range from −0.4 V to 1.2 V.

Mott–Schottky relationship expresses the potential dependence of the capacitance of space-charge layer (C_{sc}):[20,21]

$$\frac{1}{C_{SC}^2} = \frac{2}{e\varepsilon_r\varepsilon_0 N_D}\left(E - \varphi_{fb} - \frac{\kappa T}{e}\right) \quad \text{for N} - \text{type semiconductor} \quad [1]$$

$$\frac{1}{C_{SC}^2} = -\frac{2}{e\varepsilon_r\varepsilon_0 N_A}\left(E - \varphi_{fb} - \frac{\kappa T}{e}\right) \quad \text{for P} - \text{type semiconductor} \quad [2]$$

where e is electron charge (1.6×10^{-19} C), ε_r is dielectric constant of lead alloy, taken as 25 $F \cdot m^{-1}$, ε_0 is the vacuum permittivity (8.85×10^{-14} $F \cdot cm^{-1}$), N_D is the donor density, N_A is the acceptor density, E is the applied potential, φ_{fb} is flatband potential, k is Boltzmann constant (1.38×10^{-23} $J.K^{-1}$) and T is absolute temperature. N_D and N_A can be determined from the slope of the linear relationship between C_{SC}^{-2} and E, while φ_{fb} is obtained from the extrapolation to $C_{SC}^{-2} = 0$.

Raman spectroscopy.— Raman spectrum was obtained with a Jobin Yvon HR800 Raman Spectrometer system equipped with a 633 nm He-Ne laser. The power of the exciting laser measured at the sample position was about 10–25 mW. The scattered radiation from the sample passed through a SPEX Triplemate monochromator and was detected by an OMA III optical multichannel analyzer with a photodiode array thermoelectrically cooled to −35°C. The samples were pressed into self-supporting wafers. When a beam of photons strikes a molecule, the photons are scattered elastically and inelastically generating Stokes and anti-Stokes lines. Raman spectra are expressed in wave numbers which have units of inverse length. The Raman spectra of the samples were recorded at room temperature via long-focus lens for 50 times.

Results and Discussion

Effect of Cr ions on surface properties of lead alloy in the corrosion process.— As mentioned earlier, the anode performance can degrade through grain coarsening, which is highly dependent on oxide film compositions and phase structures. The growth of large grains at the expense of small grains is due to the minimization of the Gibbs free surface energy and mainly depends on the grain size and oxidation time. In order to study the microstructural development of the lead alloy oxidation films in Cr ions solution, samples with different oxidation time were prepared and their microstructure studied by SEM, EDX and XRD. The conditions of obtaining the lead alloy oxidation films are as such: CrO_3 concentration of 150 g/L, current density of 20 A/dm^2 and under room temperature (25°C) at oxidation time of 15, 30, 60 min, respectively. The SEM and EDX results of the surface oxidation layers are showed in Fig. 1. All the films contains, as expected, two kinds of grains shape, where the rod-shaped grains are determined with a composition containing Pb, Cr and O, and the ball-shaped grains of Pb and O via EDX analysis as can be seen in Fig. 1d and 1e. With the increasing oxidation time of lead alloy in CrO_3 solution, the ball-shaped grains formed on lead alloy surface grows gradually in size. Moreover, the ball-shaped grains covered gradually rods shape grains with the growth of ball shape grains. The corresponding XRD pattern of the different oxidation time in the same conditions is shown in Fig. 2. Comparing Fig. 2c with 2a and 2b, it can be found that the (120) diffraction peak of monoclinic $PbCrO_4$ are obviously weakened and the (101)/(130)/(202) diffraction peaks of lead dioxide (β-PbO_2) are strengthened remarkably in Fig. 2c. However, lead oxide diffraction peaks showed in Fig. 2 XRD patterns are relatively strong under three time constants. This indicates that the oxidation film initially consists of monoclinic $PbCrO_4$ and PbO, and then gradually β-PbO_2 forms. This is in accordance with the fact that the rod-shaped grains are mainly $PbCrO_4$ crystals and ball-shaped grains are of PbO and β-PbO_2 phases.

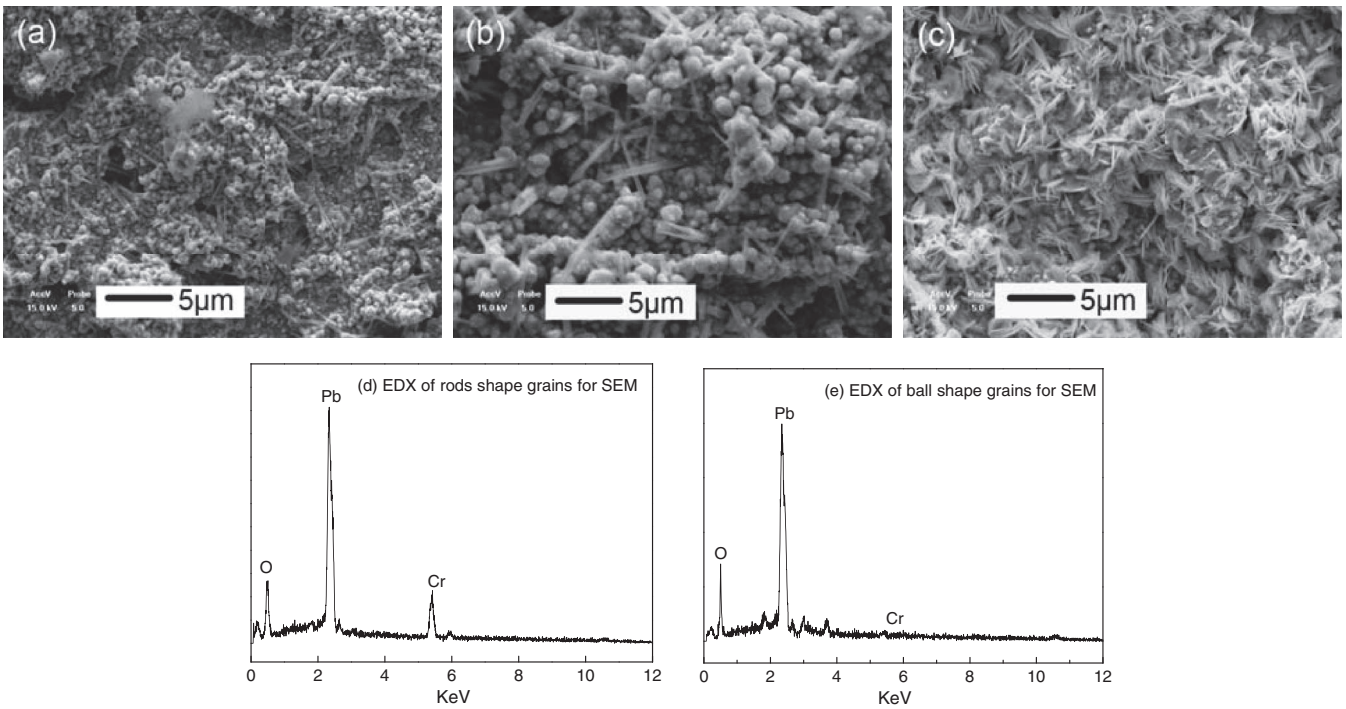

Figure 1. Surface morphology and EDX of lead alloy surface treated by electrolysis in 150 g/L CrO_3 solution under different oxidation time of (a) 15 min, (b) 30 min and (c) 60 min.

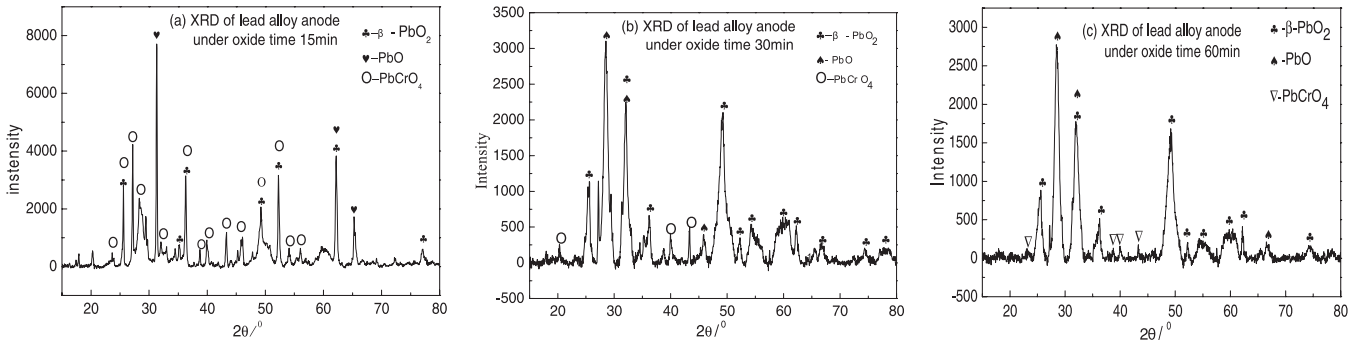

Figure 2. X-ray spectra of lead alloy surface treated by electrolysis in 150 g/L CrO_3 solution under different oxidation time of (a) 15 min, (b) 30 min and (c) 60 min.

Effect of Cr ions on electrochemistry behavior of lead alloys.— In order to further study the oxidation process between the Cr ions and the lead alloy under the presence of electric field, the electrochemical behavior of lead alloys in different CrO_3 concentration solution was examined by polarization and impedance curve measurement. Fig. 3a shows CV curves of lead alloy in CrO_3 solutions, partly enlarged image of which is showed in Fig. 3b. From Fig. 3a and 3b, the asymmetry between the oxidation and reduction processes can be seen. Anodic peaks b_1, b_2, b_3 are observed at peak potential of −0.2 V, 0.2 V and 1.3 V, respectively. Peak b_1 is believed to be corresponding to the oxidation of Pb to PbO, and b_2 the chemical reaction of Pb, PbO or $PbCrO_4$ to PbO_{1+x} ($0 < x < 1$).[22] While peak b_3 is very likely to be corresponding to the reaction to form β-PbO_2 from $PbCrO_4$, PbO_{1+x} or a little Pb. For cathodic scanning of Cr ion solution, cathodic peaks b_4 and b_5 are obviously found at peak potential of 1.35 V and −0.6 V, respectively, which should be corresponding to β-PbO_2 be reduced to $PbCrO_4$ and $PbCrO_4$ to Pb, respectively. With the increasing Cr ion concentration, anodic and cathodic peak potential remained the same, but current density corresponding to peaks of b_3 and b_4 increased. This indicates that higher CrO_3 concentrations promote β-PbO_2 formation, and significantly enhance the reduction to $PbCrO_4$.

Electrochemical impedance measurements were performed in solutions of different concentrations of CrO_3 using the lead alloy as the working electrode. The diagrams are given in Fig. 4a. In all cases, the diagram for the fixed concentrations of CrO_3 solution is characterized by one capacitive loop and one inductive loop. And three cases have been observed in a capacitive loop at high and medium frequencies, and an inductive loop at very low frequencies. High and medium frequencies loops are usually attributed to both charge transfer and the double layer associated with the interface between the electrolyte and the alloy surface. According to G. Baril et al. report,[23] these loops are the relaxation of mass transport in the growing solid oxide phase. In Fig. 4a, a clear trend is observed in the charge transfer resistance R_t (i.e., the diameter of the Nyquist curve along the real axis). The value of R_t decreases from ∼520Ω for the sample in 130 g/L CrO_3 solution to ∼300Ω for the sample in 150 g/L CrO_3 solution, and then increases to ∼330Ω for the sample in 170 g/L CrO_3 solution. This result can be explained by the fact that the corrosion production film and the adsorption ion clusters obtained in 150 g/L CrO_3 solutions present higher conductivity on the metal surface than in 130 or 170 g/L CrO_3 solutions. In addition, the polarization resistance (i.e., the difference along the real axis between the resistance at the highest and lowest frequencies) almost the same for the samples in 150 g/L and 170 g/L CrO_3 solution due to the presence of an inductive loop in the low frequency domain region of the two sample, but an increase of which is observed for 130 g/L CrO_3 solution.

In the case of low frequencies loops, the EIS results for the samples in 150 g/L and 170 g/L CrO_3 solution show a low R_t with a complete circle indicating a large inductance. For the samples in 130 g/L CrO_3 solution a larger R_t value with relatively small inductance is achieved. A. Bonnefont et al.[24] suggests that for this set of parameters one of the limiting processes is apparently the adsorption of chromium-oxide ion cluster on the free sites of the lead alloy surface. Note, however, that the mechanism giving rise to ion clusters is rather complex and the rate of another process, the surface reaction between adsorbed chromium-oxide ions cluster and lead alloy hydroxide, decreases also significantly at this modulation frequency. In addition, strong inductive loops are reported due to high concentrations of ions on relatively film-free surface.[25]

The Mott–Schottky plots obtained on lead alloy anode with different chromic anhydride concentration solution are shown in Fig. 4b. Three regions are observed in Mott–Schottky plots, where

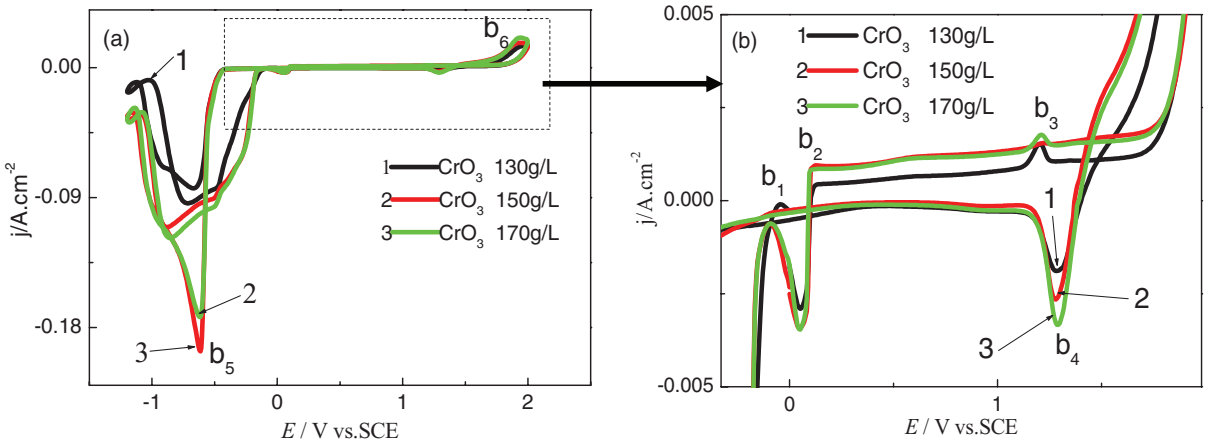

Figure 3. CV curves of lead alloy in CrO_3 solution under different concentration.

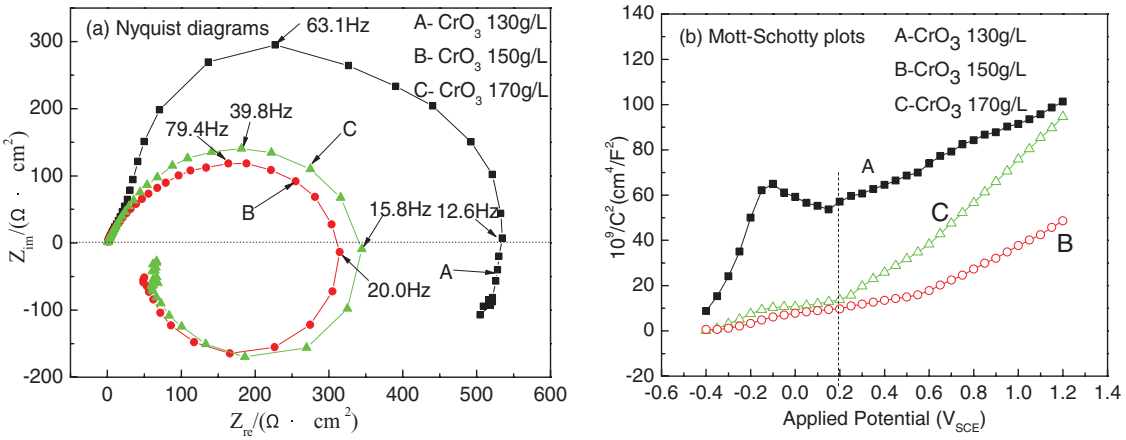

Figure 4. Nyquist diagrams and Mott–Schottky plots of lead alloy in CrO_3 solution.

one region occurred in the potential range of −0.1 V_{SCE} to 0.2 V_{SCE}, is very different from the other two regions in the potential range of −0.4 V_{SCE} to −0.1 V_{SCE}, and 0.2 V_{SCE} to 1.2 V_{SCE}, respectively. This phenomenon is attributed to the non-uniform distribution of donors in the oxidation film, which could be due to an inhomogeneous donor distribution in the oxidation film, a change in the potential of Helmholtz layer due to surface states, and the fact that two donor levels existing in the bandgap of the film. For the potential range of −0.4 V_{SCE} to 0.2 V_{SCE}, these plots are similar to those reported previously for passive films formed on stainless steels,[26] it is often assumed that the semiconducting behavior reflects the duplex characteristics of their surface oxidation films, with an inner region essentially formed of $PbCrO_4$ oxide film containing small amount of PbO, and an outer region mainly composed of PbO oxide film included minor PbO_2. Thus, in the anodic region (E< −0.1 V_{SCE}) the positive slope reveals an n-type semiconductor behavior that is characteristic of PbO. The negative slope, in the potential region 0.2 V_{SCE}> E >−0.1 V_{SCE}, results from the electrochemical behavior of a p-type semiconductor and it is related with the presence of $PbCrO_4$ in the inner oxide layers. When the potential is above 0.2 V_{SCE}, the slope is transferred to positive linear region. For an n-type semiconductor oxidation film, as identified in this work, it is suggested that the main donors are oxygen vacancies. The increase of linear slope at the transition potential implies that the donor density in oxidation film decreases, because the donor density is inversely proportional to the slope. The decrease of the concentration of oxygen vacancies at the slope-transition potential is ascribed to the oxidation of PbO in the film to PbO_2. By absorbing one unit of oxygen from water, Pb^{2+} is oxidized to Pb^{4+}. This process results directly in the increase of the concentration of oxygen vacancies in the film. Therefore, with the further increase of passive potential within the passivity range, the stability of the oxidation film is enhanced. For oxide films grown by anodization in acid solutions, however, the situation is more complex, since literature reports that the structure of oxide film on lead base alloys anode in sulphuric acid solutions is varied from $PbSO_4$, PbO or PbO_{1+x} (0 < x < 1) interface to the outer surface of α-PbO_2 or β-PbO_2.[8]

The average donor density in the oxidation film is inversely proportional to the Mott–Schottky slope is shown in Table I. It is seen that the donor densities in all cases were in the order of $10^{20}/cm^3$, indicating a highly doped semiconductor structure of the oxidation film. The highest donor density of the lead alloy is in the 150 g/L CrO_3 solution, and the lowest in 170 g/L CrO_3 solution.

The thickness (W) of the space-charge layer at a film-formation potential (E) can be calculated by:[27]

$$W = \left[\frac{2\varepsilon_r \varepsilon_0}{eN_D}\left(E - \varphi_{fb} - \frac{\kappa T}{e}\right)\right]^{1/2} \quad [3]$$

Table I. shows the thicknesses relationship of the space-charge layers in oxidation films formed on the lead alloy surfaces as function of CrO_3 solution concentration. It is seen that the space-charge layers in all cases were about 11–60 Å. The thinnest space-charge layer is in the 150 g/L CrO_3 solution.

The chemistry present in aqueous chromate solutions described as a function of chromic anhydride concentration by the following chemical equilibria is well established.[28] CrO_3 concentration above 400 g/L

$$4CrO_3 + H_2O \leftrightarrow H_2Cr_4O_{13} \quad [4]$$

$$3CrO_3 + H_2O \leftrightarrow H_2Cr_3O_{10} \quad [5]$$

CrO_3 concentration between 200∼400 g/L

$$2CrO_3 + H_2O \leftrightarrow H_2Cr_2O_7 \quad [6]$$

$$2H_2CrO_4 \leftrightarrow H_2Cr_2O_7 + H_2O \quad [7]$$

CrO_3 concentration below 200 g/L

$$CrO_3 + H_2O \leftrightarrow H_2CrO_4 \quad [8]$$

$$H_2CrO_4 \leftrightarrow H^+ + HCrO_4^- \quad [9]$$

$$2HCrO_4^- \leftrightarrow H_2O + Cr_2O_7^{2-} \quad [10]$$

for CrO_3 concentration below 200 g/L, the chromium-oxide ion clusters are essentially controlled by $HCrO_4^-$, which presents strong adsorption properties and promotes the passivation film formation. This enhances the flatband potential. When the CrO_3 concentration threshold is reached, it is assumed that the chromium-oxide ions cluster

Table I. Parameters for MS curves of lead alloy with different CrO_3 concentration solution.

CrO_3 concentration (g/L)	donor densities	flatband potential (V)	Thickness (W) of space-charge layer (Å)
130	1.26^*10^{20}	−1.056	$W = [2.2 \times 10^{-11}(E + 1.053)]^{1/2}$
150	1.43^*10^{20}	0.647	$W = [1.9 \times 10^{-11}(E - 0.650)]^{1/2}$
170	0.69^*10^{20}	0.903	$W = [4.0 \times 10^{-11}(E - 0.906)]^{1/2}$

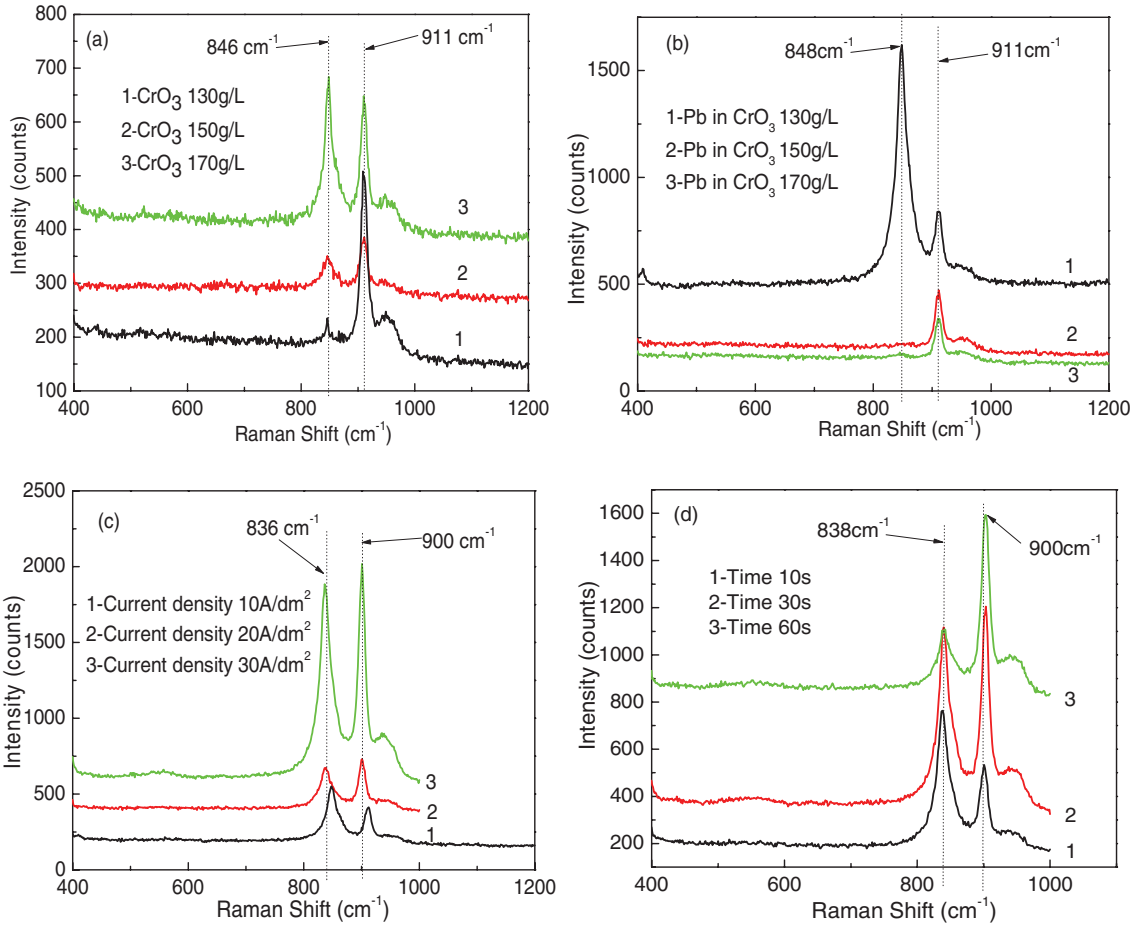

Figure 5. Raman spectra of lead alloy treated under different conditions and CrO_3 solution. (a) Raman spectra of different concentrations CrO_3 solution; (b) Raman spectra of lead alloy anode after being immersed in different concentrations of CrO_3 solution for 5s; (c) Raman spectra of lead alloy anode treated by different current density in CrO_3 150 g/L solution for 30s; (d) Raman spectra of lead alloy anode treated in CrO_3 150 g/L solution and current density of 30 A/dm^2 for different time.

forms a continuous 'sandwich' structure in aqueous chromate solutions, such that $Cr_2O_7^{2-}$ become more predominantly determined by the properties of its chromium ions, whose oxidation characteristics are greater than those of $HCrO_4^-$. This threshold can be expressed in terms of electric field strength and estimated at around 150 g/L. In terms of composition, the oxidation film on lead alloy appears to be of higher donor densities and thinner thickness (W) of space-charge layer compared with the 130 or 170 g/L CrO_3 solution.

Raman spectra of lead alloy in Cr ions solution.— The Raman spectrum of different concentrations CrO_3 solution is shown in Fig. 5a, which is dominated by two Raman bands at ~911 and ~846 cm^{-1}. These spectrums were previously assigned to terminal Cr = O vibrations of monochromate (1000 cm^{-1}) and bridging Cr-O-Cr vibrations of polychromate (845 cm^{-1}) species reported by M. M. Hoffmann et al.[28] Detection of surface chromium oxide bands of ~ 911 cm^{-1} is below bands of 1000 cm^{-1} terminal Cr = O vibrations of monochromate due to hydrogen bond absorbed by Cr = O to form Cr = O–H. Under increasing CrO_3 concentration (spectra in Fig. 5a), the decrease in the intensities of Raman bands at ~911 cm^{-1} and the increase in that of at ~846 cm^{-1} suggests that a reduction of Cr = O–H species and an enhancement of Cr-O-Cr species occurred. This shows that the band of ~846 cm^{-1} is corresponding to $Cr_2O_7^{2-}$ and the band of ~911 cm^{-1} is for $HCrO_4^-$.

After polishing, lead alloy was steeped in the different concentration of CrO_3 for 5s, and subsequently air-dried prior to Raman spectrum scanning. The Raman spectrum was used to examine the effect of the different concentration of CrO_3 solutions on chromium ions absorption on lead alloy surface. A similar set of experiments to obtain the Raman spectrum was carried out on an air-dried lead alloy surface and it can be seen that the dehydrated Raman bands at 911 cm^{-1} and ~848 cm^{-1} are nearly same with that of CrO_3 solution, compared with Fig. 5a and 5b. However, the intensities of Raman band at ~848 cm^{-1} present an obvious reduction at the concentration of the 150 and 170 g/L solutions, but is remarkably enhanced for the 130 g/L solution. These indicate that according to the wavelengths at ~846 cm^{-1} and ~911 cm^{-1} corresponding to chromium ion clusters, $Cr_2O_7^{2-}$ absorption is stronger than $HCrO_4^-$ under the low CrO_3 concentration. The reason is proposed as follows:[29] The population of chromium-oxide ions clusters on the lead alloy surface is dependent on their absorption free-energy, which is easily changed by the solution pH value. The pH value decreases with increasing the concentration of CrO_3 solution. When pH value of solution is high, adsorption free-energy of $Cr_2O_7^{2-}$ is low and $Cr_2O_7^{2-}$ is easily absorbed on the lead alloy surface. However, as the CrO_3 concentration increase, $Cr_2O_7^{2-}$ ion concentration increases. At the same time, the pH value of solution is decreased, which improves $HCrO_4^-$ adsorption. So the population of $HCrO_4^-$ adsorption increases with the increasing CrO_3 concentration, and the chromium-oxide ion adsorption is mainly controlled by the pH value of solution.

When an electrical field was introduced in CrO_3 solution with current density of 30 A/dm^2, using lead alloy as anode, the sample after oxidization time of 30s were sonicated in deionized water and subsequently air-dried. Two new Raman bands at ~836 cm^{-1} and ~900 cm^{-1} were formed on the sample surface to substitute for that at 911 cm^{-1} and ~848 cm^{-1}, as shown in Fig. 5c. The presence

of a new Raman band at ~836 cm^{-1} suggests that this band is due to a $PbCrO_4$ formation from Pb and $Cr_2O_7^{2-}$ ions. $PbCrO_4$ Raman band at ~836 cm^{-1} is similar with the $PbCrO_4$ band in E. Bandiello' studies.[30] Another new Raman at ~900 cm^{-1} corresponds to a PbO formation, which was evidenced in the initial oxidation XRD in Fig. 2. Polymerized clusters of chromium-oxide ions are readily formed in CrO_3 solution and have characteristics of electronegative ions. When electrical field was carried out in CrO_3 solution, electronegative ions are transferred along electric line of force to anode materials surface. So ions concentration on anode materials surface is higher more than the concentration if the inner solution. This changes the adsorption formation of different chromium-oxide ion clusters before and after electrical field was introduced. In addition, the action of OH^- ions is the same as chromium-oxide ions, and the pH value at the anode surface is higher than that of the inner solution. This improves the $Cr_2O_7^{2-}$ ion adsorption on the lead alloy surface. G. L. Gutsev et al.[31] have studied CrO_3 shows a very high electron affinity (EA), which indicates that it should be a strong oxidizing agent. Species with large EA's have the ability to trap free electrons in excited gases and form extremely stable negative ions, for example CrO_n^- (n = 1–5), which present the different energy feature. The low-energy decay channels of CrO_n^- anion correspond to detachment of an extra electron for n = 1–3. CrO_4^- is almost equally stable toward detachment of an extra electron or dissociation of atomic and molecular oxygen. While CrO_3^- is rather stable toward detachment of an extra electron and dissociation of an atomic oxygen, it is much less stable with molecular oxygen. CrO_3^- readily bond with superoxo O_2 to form CrO_5^-. This deduce that $PbCrO_4$ formation under condition of electric field is via reaction of

$$Cr_2O_7^{2-} \rightarrow CrO_5^- + CrO_2^- \quad [11]$$

$$2CrO_5^- + 2Pb \rightarrow 2PbCrO_4 + O_2 + 2e \quad [12]$$

For PbO species, its formation is supposed to be through the following reactions:

$$2HCrO_4^- \rightarrow 2CrO_3^- + H_2O + O \quad [13]$$

$$CrO_3^- \rightarrow CrO_2^- + O \quad [14]$$

$$2Pb + 2O \rightarrow 2PbO \quad [15]$$

CrO_2^- ions released from reaction 11 and reaction 14 are reacted with OH^- ions at the anode surface:

$$2CrO_2^- + 4OH^- \rightarrow 2CrO_4^{2-} + 4H^+ + 6e \quad [16]$$

To examine the changes to the surface properties of lead alloy in the initial oxidation stage, Raman spectrums analyzes were performed again. These analyzes were carried out on samples that where oxidized by different current density in CrO_3 150 g/L solution for 30s, and treated in CrO_3 150 g/L solution and current density of 30 A/dm^2 for different time. The Raman spectra results are shown in Fig. 5c and 5d. As can be seen, the Raman bands intensity ratio of ~900 cm^{-1} to ~836 cm^{-1} appears to increase with an increase of current density (See Fig. 5c) and oxidation time (See Fig. 5d). This reveals that the oxidation film compositions are dominated by PbO or β-PbO_2, not $PbCrO_4$. The reasons are that the oxidation extent of the lead-alloy anode increases with an increase in current density and oxidation time, which are showed in reactions 12–14, to promote the formation of PbO or β-PbO_2. These results are in accordance with the oxidation film compositions of lead alloy for longer oxidation time observed in XRD spectra.

Conclusions

At the initial oxidation stage of the Pb-3 wt%Sn-0.5 wt%Ag anode, the diffraction peaks of monoclinic $PbCrO_4$ are obviously found. With increasing oxidation times, $PbCrO_4$ diffraction peaks weakened and the diffraction peaks of lead dioxide (β-PbO_2) are strengthened remarkably from lead oxide (PbO) indicating the oxidation film compositions are mainly PbO or β-PbO_2.

Cyclic voltametric measurements revealed that the formation of PbO is of lower electrode potential, deeply with oxidation reaction to develop into PbO_{1+x} ($0 < x < 1$) and then to form β-PbO_2. This routine does not change in CrO_3 solutions of different concentrations. According to AC impedance tests, charge transfer and a corrosion production film on the lead alloy surface happen under the high and medium frequency of electric field, and chromium-oxide ion clusters are absorbed on lead alloy surface free sites for low frequency. But the corrosion product have characteristics of complex semiconducting behavior shown in Mott–Schottky plots. In the potential region $E < -0.1\ V_{SCE}$ or $E > 0.2\ V_{SCE}$, the positive slope reveals an n-type semiconductor behavior that is characteristic of PbO or β-PbO_2. The negative slope, in the potential region $0.2\ V_{SCE} > E > -0.3\ V_{SCE}$, results from the electrochemical behavior of a p-type semiconductor and it is related to the presence of $PbCrO_4$ in the inner oxide layers. Based on the relationship of the thicknesses of the space-charge layers, their thickness in all cases were calculated to be within 11–60 Å.

From the observation in Raman spectra of lead alloy and CrO_3 solution, $Cr_2O_7^{2-}$ with a band at 848 cm^{-1} and $HCrO_4^-$ with a band at 911 cm^{-1} are firstly absorbed on anode surface. $PbCrO_4$ is then produced from a reaction between $Cr_2O_7^{2-}$ and Pb and PbO is produced from a reaction between $HCrO_4^-$ and Pb. With a longer oxidation time and a higher current density, population of atomic or molecular oxygen is remarkably enhanced, and consequently the formation of PbO and PbO_2 is promoted.

Acknowledgments

This work was financially supported by the National Natural Science Foundation of China (51004028) and the Special Fund for Basic Scientific Research of Central Colleges (N100402002).

References

1. I. Ivanov, Y. Stefanov, Z. Noncheva, M. Petrova, Ts. Dobrev, L. Mirkova, R. Vermeersch, and J.-P. Demaerel, *Hydrometallurgy*, **57**, 109 (2000).
2. F. A. Pérez-González, C. G. Camurri, C. A. Carrasco, and R. Colás, *Materials Characterization*, **64**, 62 (2012).
3. D. Devilliers, M. T. Dinh Thi, E. Mahé, and Q. Le Xuan, *Electrochim. Acta*, **48**, 4301 (2003).
4. N. Li, J. S. Zhang, B. H. Sencer, and D. Koury, *Nuclear Instruments and Methods in Physics Research A*, **562**, 695 (2006).
5. D. R. P. Egan, C. T. J. Low, and F. C. Walsh, *J. Power Sources*, **196**, 5725 (2011).
6. W. R. Osório, L. C. Peixoto, and A. Garcia, *J. Power Sources*, **194**, 1120 (2009).
7. Y. Li, L. X. Jiang, X. J. Lv, Y. Q. Lai, H. L. Zhang, J. Li, and Y. X. Liu, *Hydrometallurgy*, **109**, 252 (2011).
8. A. M. Lafront, W. Zhang, E. Ghali, and G. Houlachi, *Electrochim. Acta*, **55**, 6665 (2010).
9. C. Rerolle and R. Wiart, *Electrochim. Acta*, **41**, 1063 (1996).
10. I. Ivanov, Y. Stefanov, Z. Noncheva, M. Petrova, Ts. Dobrev, L. Mirkova, R. Vermeersch, and J.-P. Demaerel, *Hydrometallurgy*, **57**,125 (2000).
11. W. Zhang and G. Houlachi, *Hydrometallurgy*, **104**, 129 (2010).
12. Y. Q. Lai, L. X. Jiang, J. Li, S. P. Zhong, X. J. Lü, H. J. Peng, and Y. X. Liu, *Hydrometallurgy*, **102**, 73 (2010).
13. D. G. Li, G. S. Zhou, J. Zhang, and M. S. Zheng, *Electrochim. Acta*, **52**, 2146 (2007).
14. T. Hirasawa, K. Sasaki, M. Taguchi, and H. Kaneko, *J. Power Sources*, **85**, 44 (2000).
15. J. Xu, X. B. Liu, X. G. Li, E. Barbero, and C. F. Dong, *J. Power Sources*, **155**, 420 (2006).
16. E. M. Baker and P. J. Merkus, *J. Electrochem. Soc.*, **61**, 327 (1932).
17. F. Hine, K. Takayasu, and N. Koyanagi, *J. Electrochem. Soc.*, **133**, 346 (1986).
18. M. J. P. Mcburney and D. R. Gabe, *Surf. Tech.*, **9**, 253 (1979).
19. L. Lu, T. C. Liu, and X. G. Li, *Surf. Coat. Tech.*, **202**, 1401 (2008).
20. L. V. Taveira, M. F. Montemor, M. Da Cunha Belo, M. G. Ferreira, and L. F. P. Dick, *Corros. Sci.*, **52**, 2813 (2010).
21. K. Darowicki, S. Krakowiak, and P. Slepski, *Electrochim. Acta*, **51**, 2204 (2006).
22. D. G. Li, D. R. Chen, J. D. Wang, and H. S. Chen, *J. Power. Sources*, **196**, 8789 (2011).
23. G. Baril, C. Blanc, M. Keddam, and N. Pébère, *J. Electrochem. Soc.*, **150**, B488 (2003).
24. A. Bonnefont, R. Morschl, P. Bauer, and K. Krischer, *Electrochim. Acta*, **55**, 410 (2009).

25. G. Baril, G. Galicia, C. Deslouis, N. Pebere, B. Tribollet, and V. Vivier, *J. Electrochem. Soc.*, **154**, C108 (2007).
26. H. X. Guo, B. T. Lu, and J. L. Luo, *Electrochim. Acta*, **52**, 1108 (2006).
27. G. A. Zhang and Y. F. Cheng, *Electrochimica Acta*, **55**, 316 (2009).
28. M. M. Hoffmann, J. G. Darab, and J. L. Fulton, *J. Phys. Chem. A*, **105**, 1772 (2001).
29. S. R. Chowdhury, E. K. Yanful, and A. R. Pratt, *J. Hazardous Materials*, **235**, 246 (2012).
30. E. Bandiello, D. Errandonea, D. Martinez-Garcia, D. Santamaria-Perez, and F. J. Manjón, *Physical Review B*, **85**, 1 (2012).
31. G. L. Gutsev, P. Jena, H. J. Zhai, and L. S. Wang, *J. Chem. Phys.*, **115**, 7935 (2001).